Earth and Planetary Science Letters 602 (2023) 117971

Contents lists available at ScienceDirect

Earth and Planetary Science Letters

journal homepage: www.elsevier.com/locate/epsl

Shear-induced distortion of clay minerals aids in dynamic weakening of shallow faults during earthquakes

Bowen Yu, Lu Yao *, Shengli Ma, Weifeng Qin

State Key Laboratory of Earthquake Dynamics, Institute of Geology, China Earthquake Administration, Beijing 100029, China

ARTICLE INFO

Article history:
Received 30 June 2022
Received in revised form 29 November 2022
Accepted 16 December 2022
Available online 4 January 2023
Editor: R. Bendick

Keywords:
dynamic fault weakening
mechanochemical effect
flash heating
thermochemical pressurization
characteristic weakening temperature
thermal decomposition

ABSTRACT

Coseismic faulting may activate complicated physicochemical processes in the fault zone through both mechanical deformation and frictional heating. While plenty of work emphasizes the great importance of thermal effects on dynamic fault weakening, less attention has been paid to the mechanochemical effects. We study the effects of mechanochemical changes of chlorite on its dynamic weakening process via low- and high-velocity friction experiments, simultaneous thermal analysis, X-ray diffraction, microstructural observation, and numerical modeling in this work. With higher degrees of deformation, the experimentally sheared chlorite samples generally show more pronounced reductions in the onset temperature of thermal decomposition (T_{d0}; from 561 °C to 189 °C in the extreme case) and more striking increases in the reaction rate. The exponential-decay formula can well describe the relation between T_{d0} and the mechanical work (integral of shear stress with respect to displacement) in the shear deformation. Moreover, the presence of pore water and the variation in chlorite content could significantly affect the mechanochemical changes of the sheared chlorite-bearing samples. Taking the markedly lowered T_{d0} as the characteristic temperature leading to thermal softening of asperity contacts, numerical modeling shows that flash weakening of chlorite-rich samples can be significantly promoted, dwarfing the thermochemical pressurization that is also enhanced by mechanochemical effects though. This is largely supported by high-velocity experiments (~m/s) performed on the pre-deformed chlorite samples, which show both lower peak friction and fracture energy, and earlier activation of dynamic weakening. Clearly, shear deformation plays a key role in aiding thermally-activated mechanisms in weakening faults and facilitating rupture propagation during earthquakes.

1. Introduction

Theoretical analysis and numerical modeling have demonstrated that dynamic weakening of faults during earthquakes can promote seismic rupture propagation and aggravate earthquake disasters (Noda and Lapusta, 2010, 2013; Rice, 2006). In the past three decades, high-velocity rock friction experiments have improved our understanding of dynamic fault weakening mechanisms (Di Toro et al., 2011; Tullis, 2015; Shimamoto and Tsutsumi, 1994). The experimental studies have revealed close connections between coseismic fault weakening and physicochemical changes of fault-zone materials. Besides the prominent examples like melt and gel lubrication, more weakening mechanisms show such connections. For instance, flash heating is controlled by thermal melting, or more generally, thermal softening of asperity contacts (Beeler et al., 2008; Goldsby and Tullis, 2011; Kohli et al., 2011; Rice, 2006; Tisato et al., 2012), and thermochemical pressurization (e.g., Brantut et al., 2010; Sulem and Famin, 2009; Tanikawa et al., 2009) is driven by thermally-activated reactions that release fluids.

Seismic slip at the velocity of ~m/s during earthquakes could bring about severe deformation of fault-zone materials in addition to rapid frictional heating (e.g., Kaneki et al., 2020). According to the basic principle of thermodynamics, high mechanical work input into slip zones may assist frictional heating in triggering physicochemical changes of slip-zone materials. This is clearly demonstrated by Hirono et al. (2013) and Kim et al. (2021), where they revealed that the deformed illite or dolomite might have lower activation energy of decomposition reactions. Kim et al. (2021) also reported a reduction in the onset temperature of thermal decarbonation of dolomite by ~200 °C due to mechanical deformation. By using the kinetic parameters of thermal decomposition determined for the deformed samples, numerical modeling in these studies suggest that the efficiency of thermochemical pressurization can be enhanced. However, the use of the intrinsic friction coefficient of 0.1–0.2 in the numerical modeling of these

* Corresponding author.
E-mail addresses: yaolu_cug@163.com, luyao@ies.ac.cn (L. Yao).

https://doi.org/10.1016/j.epsl.2022.117971
0012-821X/

studies naturally means that other mechanisms may play a major role in fault weakening, besides the enhanced thermochemical pressurization. As coseismic fault weakening is closely linked with physicochemical changes of fault-zone materials (Di Toro et al., 2011; Tullis, 2015), from a wider perspective, we may expect that the mechanochemical changes of slip-zone materials could affect other fault weakening mechanisms such as flash weakening, which is thought to be efficient in the inception of coseismic fault slip.

In the seminal work of Rice (2006) that proposes flash heating model, the characteristic weakening temperature (T_w) required to degrade the strength of asperities is assumed to be submelting temperature. Experimental and microstructural constraints on the exact processes relevant to the weakening of asperity contacts are still lacking. How can we estimate T_w is thus debatable even for the thermally stable rocks. As discussed in Rice (2006) and Beeler et al. (2008), the degradation of asperity strength may occur at submelting temperature (Molinari et al., 1999), and the release of water due to the breakdown of hydrous phases in rocks could generally lower the melting point of rocks. When applying the flash weakening model to thermally unstable rocks, many previous workers suggest that T_w could correspond to the temperature of thermal decomposition or phase transition (e.g., Kohli et al., 2011; Tisato et al., 2012; Tullis, 2015). For instance, in the analysis of flash weakening in limestone and serpentinite, the decarbonation temperature of calcite and the dehydration temperature of antigorite are considered as T_w, respectively (Kohli et al., 2011; Tisato et al., 2012). The physical basis of asperity weakening associated with thermal decomposition seems not to be as obvious as that in the case of local asperity melting. Little is currently known about how the weight loss and volume reduction amid the decomposition reactions may affect the strength of asperities. Previous work suggests that the formation of weak phases by thermal decomposition may provide the likely basis (e.g., amorphous carbon for carbonates and talc for serpentinite; Spagnuolo et al., 2015; Kohli et al., 2011). Moreover, friction experiments performed under room temperature and humidity suggest that a thin layer of water adsorbed on gouge particles may reduce fault friction dramatically at subseismic slip rates (Reches and Lockner, 2010; Sammis et al., 2011). For hydrous phyllosilicates, whether the thermally released water may lubricate the asperity contacts or enhance the viscous deformation (e.g. Pozzi et al., 2021) on the contacts during rapid slip are also open questions.

The shallow regions of faults often abound in clay minerals and favor stable slip (Scholz, 2002), whereas coseismic fault weakening may enable earthquake rupture to break through these regions, as suggested by both numerical modeling and lab experiments (Noda and Lapusta, 2013; Rubino et al., 2022). Understanding the dynamic weakening processes of common clay minerals is thus crucial for comprehending the development of surface rupture in natural and induced earthquakes, with great importance to the assessment of seismic hazards. Hirono et al. (2013) have shown that the mechanochemical changes of the sheared illite may promote its dynamic weakening through thermochemical pressurization. In this work, we explore whether shear deformation may affect flash weakening and thermochemical pressurization in chlorite. The main reason we select chlorite as a representative sample lies in its common occurrence in sedimentary, metamorphic and igneous rocks over a wide range of temperature and pressure conditions (e.g., Bourdelle and Cathelineau, 2015).

In this study, we use simultaneous thermal analysis (STA: thermogravimetry (TG) plus differential scanning calorimetry (DSC) analysis) to examine mechanochemical changes of chlorite and chlorite-bearing gouges retrieved from friction experiments under a slip rate of 1.0 mm/s and different normal stresses, shear displacements, and fluid conditions. X-ray diffraction (XRD) analysis and microstructural observations are used to decipher the TG/DSC results. These together with numerical modeling and comparative experiments performed at high slip velocities (~0.5 to 1.0 m/s) suggest that shear distortion of chlorite may promote dynamic weakening of chlorite-rich samples efficiently through flash heating.

2. Materials and methods

2.1. Friction experiments

Friction experiments were performed on chlorite and chlorite-quartz mixtures using a low- to high-velocity rotary shear apparatus at the Institute of Geology, China Earthquake Administration (Ma et al., 2014; see sample assemblies in Fig. S1). The chlorite sample was prepared from chlorite schist containing >96% clinochlore (crystallochemical formula ($K_{0.004}Na_{0.007}Ca_{0.002}Mg_{3.756}Mn_{0.005}Fe^{2+}_{0.895}Al^{VI}_{1.328}Ti_{0.004}$)[($Al^{IV}_{1.326}Si_{2.674}$)$O_{10}$]$(OH)_8$). The quartz sample commercially available was used to prepare three kinds of chlorite-quartz mixtures with 20 wt%, 50 wt% and 80 wt% chlorite, respectively. Grain sizes of all the samples were controlled to be less than 75 μm using a 200# sieve. The inner and outer diameters of the ring-shaped gouge layer are 22 and 30 mm, respectively, and the gouge thickness is about 1.5 mm. To evaluate how shear deformation may affect the thermally-activated weakening mechanisms, we have to isolate the effects of deformation from the thermal effects. The slip rate (V) of 1 mm/s was thus adopted in most of the tests to impose shear deformation on the samples without involving the effects of frictional heating (temperature measurement and numerical modeling suggest that the highest temperature within the gouge layer in all our experiments performed at V = 1 mm/s may not exceed 80 °C). For these low-velocity friction experiments, the normal stress (σ_n) and displacement (d) ranged from 5 to 40 MPa and 0.2 to 5 m, respectively. Here both V and d are equivalent values for the ring-shaped or circular slip surfaces as introduced in Shimamoto and Tsutsumi (1994). The pore fluid conditions included room humidity and pore water pressure of 1 MPa (hereafter referred to as dry and wet conditions). Several high-velocity friction experiments were performed at slip rates of 0.5 or 1.0 m/s and normal stress of 1.0 MPa under room humidity. The samples used in high-velocity tests include undeformed and pre-deformed (prepared by a planetary ball mill) chlorite and quartz-chlorite mixture. Details of the sample assembly and the experimental conditions can be found in Supplemental Material.

2.2. STA and XRD analysis

After each experiment, we collected some pieces of the deformed gouge for microstructural observation and mixed the rest uniformly to perform STA and XRD analysis. The STA analysis was conducted in a Netzsch 449F3 thermal analyzer equipped with a rhodium furnace, following the procedures suggested by Netzsch (Arkhangel'Skii et al., 2013) and many previous studies (e.g., Hirono and Tanikawa, 2011). About 8 mg sheared samples were placed in a Pt-Rh crucible and heated following a predefined heating procedure, which includes 1) heating the sample from room temperature to 80 °C; 2) keeping the temperature at 80 °C for 12 min to eliminate the absorbed water; 3) heating the sample from 80 °C to 1050 °C at a constant heating rate of 5–20 °C/min. These heating rates and the sample amount in our STA analysis are comparable to those in previous studies (e.g., Hirono and Tanikawa, 2011). Although the chemistry community recommends that the sample mass times heating rate should not exceed 100 mg°C/min (Vyazovkin et al., 2014), the heterogeneity of fault rocks (thus higher sample mass may improve the reliability of the analysis) and the rapid frictional heating during coseismic slip suggest that we may not have to strictly follow such a criterion when we

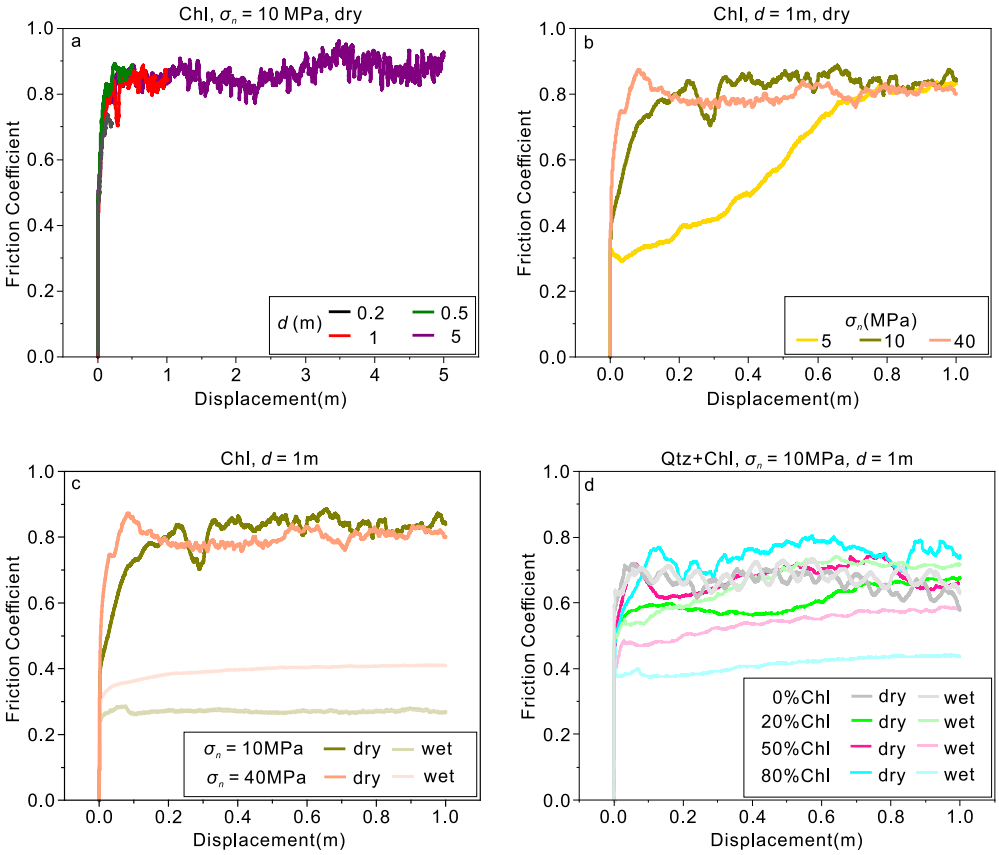

Fig. 1. Mechanical data from experiments conducted on chlorite, quartz and chlorite-quartz mixtures under a slip rate (V) of 1 mm/s, and various displacements (d), normal stresses (σ_n) and environmental conditions (room-humidity (dry) or water-saturated with a pore pressure of 1 MPa (wet)). (a), Chlorite, σ_n = 10 MPa, d = 0.2–5 m; dry. (b), Chlorite, σ_n = 5–40 MPa, d = 1 m; dry. (c), Chlorite, σ_n = 10 and 40 MPa, d = 1 m; dry and wet; (d), Pure quartz or chlorite-quartz mixtures, σ_n = 10 MPa, d = 1 m; dry and wet. (For interpretation of the colors in the figure(s), the reader is referred to the web version of this article.)

study coseismic faulting. The TG data collected under the various heating rates were used in the kinetic analysis.

The XRD analysis was performed using a Bruker D8A A25 X spectrometer. As we may expect the distortion of chlorite crystal structures and the formation of amorphous materials in the experimentally-sheared samples (Hirono et al., 2013; Kaneki et al., 2020), the changes in the intensity of characteristic peaks and the crystallinity of chlorite are our primary concerns. We thus mix 20% corundum (Al_2O_3) powder into the sheared samples in the analysis and take the corundum as an internal standard. The XRD patterns were collected over the 2θ range of 4–75°, with the step size of 0.02° and the scanning rate of 4 °/min.

3. Results

3.1. Friction experiments at slip velocity of 1 mm/s

Fig. 1 shows the evolution of friction coefficient (μ) with slip displacement (d) under various experimental conditions. For the tests on the dry chlorite gouge under σ_n = 10 MPa and d = 0.2–5 m or σ_n = 5–40 MPa and d = 1 m, the steady-state friction coefficients (μ_{ss}) reach roughly the same level of 0.71–0.83 (Figs. 1a and b), albeit the μ evolution towards μ_{ss} may be different probably due to the difference in initial compaction status. The wet chlorite gouge exhibits much lower μ_{ss} of 0.27–0.41 under σ_n = 10 and 40 MPa (Fig. 1c). For the chlorite-quartz mixture gouge, μ_{ss} decreases with increasing chlorite contents under the wet condition (light-colored lines in Fig. 1d), while the relation between chlorite content and μ_{ss} under the dry condition is indistinguishable among the tests (Fig. 1d).

3.2. STA and XRD analysis

Figs. 2a–d show TG profiles of the samples retrieved from the friction experiments exhibited in Figs. 1a–d, respectively. The measurement conditions adopted in the thermal analysis of each sample are exactly the same. The plots of the characteristic temperature of thermal decomposition (T_d), which is defined as the temperature corresponding to a given reacted fraction of chlorite (α) determined from the TG data, are displayed in Figs. 3a–d. As a reference, the original chlorite (undeformed) starts to decompose at about 561 °C (α = 0.05). By contrast, the sheared chlorites have much lower T_d and faster weight loss with increasing displacements and normal stresses adopted in the friction experiments (Figs. 2a–b and 3a–b). The T_d at α = 0.05–0.9 vary a lot among the samples sheared under different conditions, especially for α < 0.4 (e.g., the difference in T_d at α = 0.05 can be as large as 377 °C; Figs. 3a–b). For a given normal stress, the weight loss is generally faster and T_d is lower for the chlorite sheared under the dry condition, as compared to that sheared under the wet condition (Figs. 2c and 3c). The same trend can be observed for the chlorite-quartz mixture with 80% chlorite, but this is not the case for the mixture with 20% chlorite (Figs. 2d and 3d). The simultaneously measured DSC data are displayed in Fig. S3 in Supplemental Material, which are mainly used to calculate the enthalpy of the thermal decomposition reaction required in the numerical modeling of thermochemical pressurization.

In XRD analysis, each XRD pattern was normalized so that the characteristic peak of the mixed corundum (20 wt.%) at 2θ = 57.5° had an intensity of 1000 cps. We also calculated the chlorite crystallinity ([(area under the crystalline peaks)/(area under all

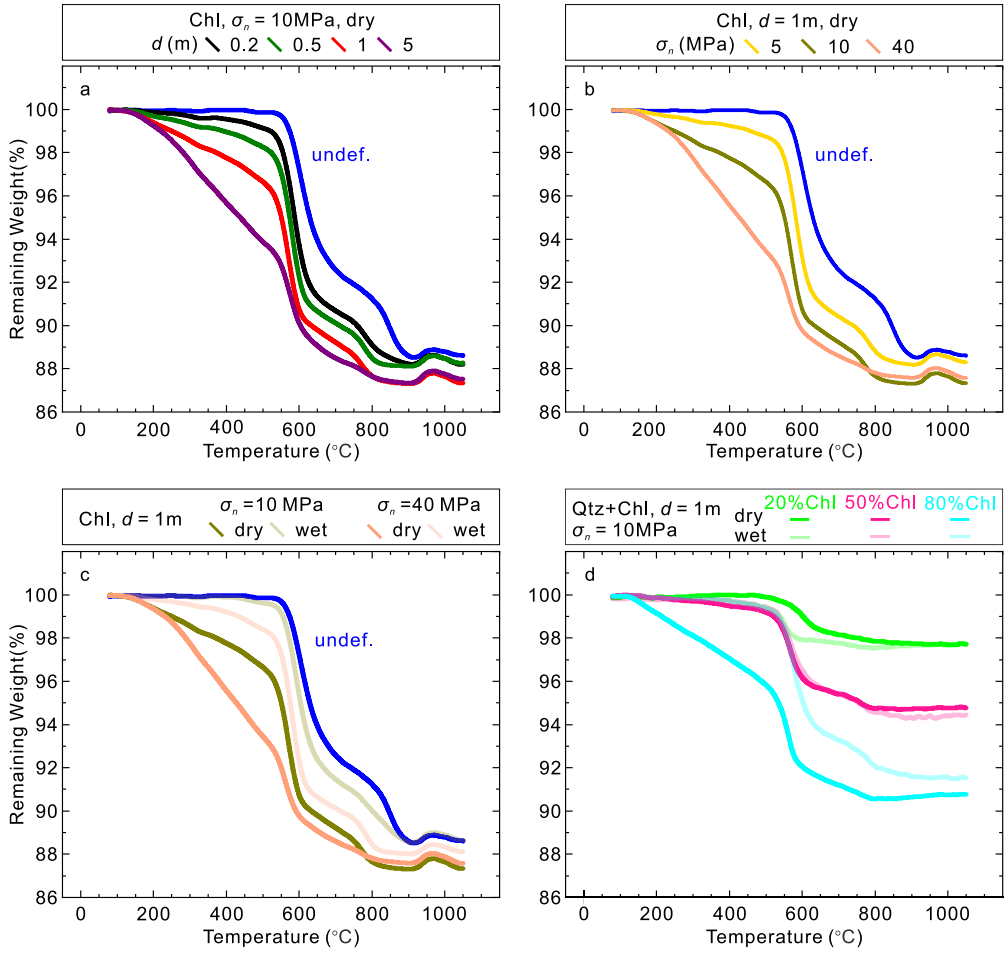

Fig. 2. Thermogravimetry (TG) profiles of the sheared gouges recovered from the friction experiments as shown in Figs. 1a–d. The heating rate was 20 °C/min for all the TG data shown here. Colors of lines and symbols in each figure denote the conditions of the friction experiments. σ_n: normal stress, d: displacement. (For interpretation of the colors in the figure(s), the reader is referred to the web version of this article.)

peaks)*100]) in the sheared samples (see details in Supplemental Material). For the chlorite gouges sheared under the dry condition, we can observe gradual decreases in the peak intensity and the crystallinity of chlorite with increasing normal stresses and shear displacements in the friction experiments (Figs. 4a–b, and Figs. S4a and S4b in Supplemental Material). The presence of pore water in the friction experiments helps maintain high peak intensity and crystallinity of chlorite as compared to the dry cases (Fig. 4c and Fig. S4c). This is also true for the chlorite-quartz mixtures with 50–80% chlorite, but tends to become the opposite for the mixture containing 20% chlorite (Fig. 4d).

3.3. Microstructures

For the dry chlorite sheared at σ_n = 10 MPa and d = 0.5–1.0 m, the deformation textures (Figs. 5a and 5b) are featured by the formation of shear bands composed of comminuted chlorite (enclosed by dashed lines), and the development of Riedel (R) and Y shears. Increases in d and σ_n lead to thicker shear bands (150 versus 410 μm for d = 0.5 and 1.0 m, respectively; Figs. 5a and 5b; Fig. S7b–c). An intriguing observation is that the chlorite gouges deformed under the wet condition yield totally different shear textures—most of the chlorites align in the directions of Y- and R-shears without severe distortion and comminution (cp. Fig. 5c and Fig. S7a). Shear deformation in this case might be mainly accommodated by multiple localized shear planes (LSP) developed along some Y- and R-shears (see LSP marked in Fig. 5c, some of which are straight and continuous).

For the chlorite-quartz mixtures with 20% chlorite, thicker shear band can be observed under the wet condition (cp. Figs. 5d–e). With chlorite content going up to 80%, severe comminution can be observed in a wide shear band under the dry condition, as compared to the existence of weakly or undeformed chlorite flakes and the development of multiple localized shear bands/planes under the wet condition (cp. Figs. 5f–g).

4. Discussion

4.1. Mechanochemical changes of chlorite under various conditions

In this study, we evaluate a few potential factors (e.g. normal stress, shear displacement, fluid condition and chlorite content) that may affect the mechanochemical changes of chlorite subjected to shear deformation. The results from STA, XRD and microstructural analysis of the deformed samples are mutually consistent. In general, higher degrees of shear deformation and more intense distortion of chlorite are more likely to expedite its decomposition reaction, in accord with previous studies on illite and dolomite (Hirono et al., 2013; Kim et al., 2021). Impressive observations are that both the deformed dolomite (Kim et al., 2021) and chlorite (this study) have significantly lowered onset temperatures of thermal decomposition (from 561 °C to ~189 °C for chlorite in the extreme case), which may have crucial implications for the flash weakening of faults as discussed later.

For the purpose of possible application of the experimental results to natural faults, we compile the TG and T_d data, and analyze

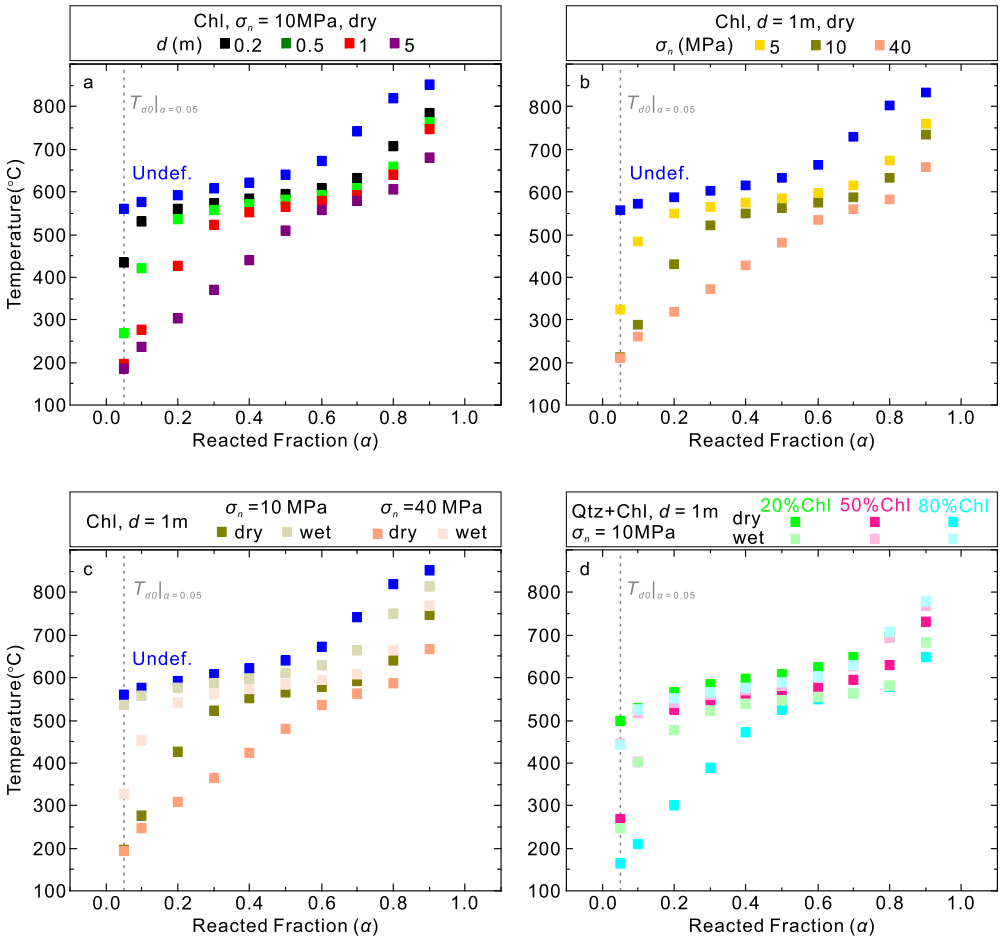

Fig. 3. Characteristic temperature of thermal decomposition (T_d) extracted from TG profiles shown in Fig. 2. T_d is defined as the temperature at which thermal decomposition of chlorite reaches a given fraction. σ_n: normal stress, d: displacement. (For interpretation of the colors in the figure(s), the reader is referred to the web version of this article.)

how these may change with the mechanical work done in the friction experiments (M, integral of shear stress with respect to displacement). The TG data reveal that thermal decomposition of the pre-sheared chlorite can be overall expedited with increasing M (Fig. 6a). T_{d0}, which is defined as the characteristic temperature at which the reacted fraction α = 0.05, is plotted against M in Fig. 6b. The T_{d0} decreases exponentially with M, which can be fitted with the following equation:

$$T_{d0}(M) = T_{d0\_inf} + \left(T_{d0\_und} - T_{d0\_inf}\right)\exp(-bM), \quad (1)$$

where T_{d0_und} and T_{d0_inf} are T_{d0} values for the undeformed sample (561 °C; obtainable from the TG data) and the pre-deformed sample with infinitely high M, respectively, and b is a positive constant. The data fitting to Eq. (1) yields T_{d0_inf} = 180 °C and b = 2.8e-7.

Previous studies suggest that thermal decomposition of the undeformed chlorite includes two distinct dehydroxylation steps (Földvári, 2011; Steudel et al., 2016). For iron-free clinochlore, three water molecules are released from the interlayer octahedral sheet between 400–700 °C in the first step (556–743 °C in our measurement), and another one water molecule is released from the 2:1 layers between 600 and 900 °C in the second step (810–894 °C in our measurement), with the possible formation of forsterite, enstatite, and spinel at last (Steudel et al., 2016). We calculated the activation energy (E_a) of the undeformed and deformed chlorite samples (recovered from three typical experiments) based on Friedman analysis (Friedman, 1964). The determined E_a varies a lot at α = 0.05–0.9 for both the undeformed and deformed samples (Fig. S6), suggesting the existence of multiple reaction steps. The E_a of the undeformed sample ranges from 57.58 to 497.93 kJ/mol at different α, with an average value of 283 kJ/mol, which is higher than the E_a of 197 kJ/mol for the Fe-bearing chlorite reported in Masumoto et al. (2018). This might be attributed to the different types of chlorite used in the two studies, as suggested by the distinct TG results (cp. Fig. 5b in Masumoto et al. (2018) and the Fig. 2 in this study). For the chlorite samples deformed under dry and wet conditions, the E_a at α < 0.4 could be either significantly (dry) or slightly (wet) lower than that of the undeformed sample. The corresponding average E_a are 139 kJ/mol and 241 kJ/mol, respectively, over the α of 0.05–0.9. These results suggest that the first dehydroxylation process can be activated at a temperature lower than <200 °C with reduced E_a (Fig. S6 in Supplemental Material) when chlorite experiences intensive shear deformation. The underlying mechanism(s) cannot be well constrained by the data we collected. The likely causes may include the grain size reduction (surface energy increase) and the distortion of the crystal structure of chlorite. We actually have conducted similar studies on several other thermally-unstable minerals. It turns out that shear deformation may not always induce significant mechanochemical changes of the minerals (e.g., calcite as a counterexample), despite the fact that the grain sizes always reduce dramatically after friction experiments. We thus believe that the distortion of the crystal structure of minerals is likely a major cause. The easier distortion of the crystal structure, the

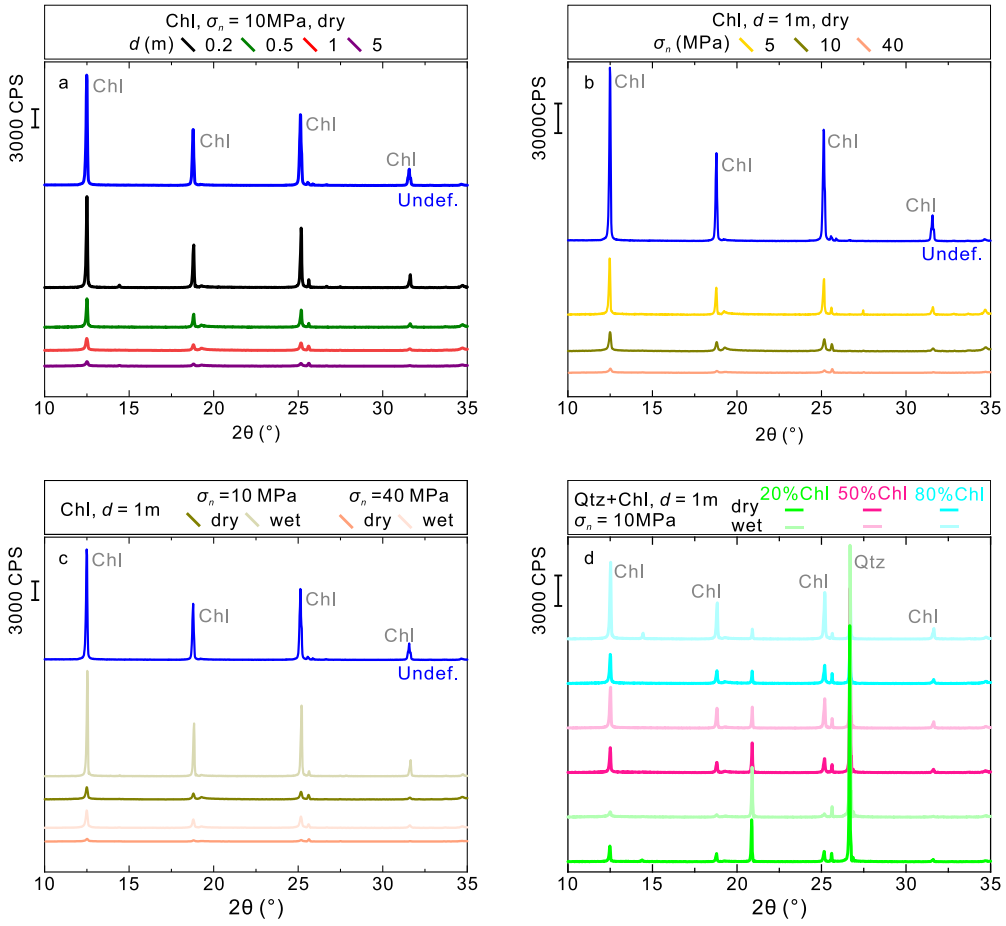

Fig. 4. X-ray diffraction (XRD) patterns of the sheared gouges recovered from the friction experiments as shown in Figs. 1a–d. The pattern of the undeformed chlorite sample is plotted in (a)–(c) for comparison. (For interpretation of the colors in the figure(s), the reader is referred to the web version of this article.)

greater mechanochemical changes of the minerals might be. More detailed work needs to be done to solve the mystery in the future.

Pore water and chlorite content could impact the mechanochemical changes of chlorite-bearing samples. For the samples containing $\geq$ 80% chlorite, the presence of pore water can lead to the formation of multiple localized shear bands (Figs. 5c and 5g) and thus prevent the bulk chlorite layer from shear deformation and mechanochemical changes (Figs. 2c and 2d). However, when the chlorite content reduces to 20 wt%, more materials tend to be involved in the intense shear under the wet condition (cp. Figs. 5d and 5e) and the mechanochemical changes of chlorite are thus more obvious (Fig. 2d). All these results suggest the complexities of the mechanochemical changes of chlorite-rich fault zones during seismic slip (probably applicable to the cases of other thermally-unstable rocks). Essentially, the mechanochemical changes of minerals could be closely linked to their deformation textures (e.g., the degree of shear localization and the volume involved). If shear deformation is very localized during seismic slip (like the case in some of the wet experiments), the shear-enhanced thermochemical pressurization may become less important. The reason is that the volume of the reactant with the lowered onset temperature and activation energy of decomposition reaction could be tiny in the case of highly localized shear, adding minor contribution to expediting pore pressure rise. However, even in such a case, flash weakening of faults still can be significantly promoted, as discussed below in section 4.2.

As shear localization could be remarkable in many of our experiments, one may question to what extent the mechanochemical changes of the uniformly mixed samples may reflect those of the highly-sheared slip zones. It is likely that the former may underestimate the latter. The reason why we didn't perform STA and XRD analysis on the slip-zone materials lies in that separating these of several microns to a few hundred microns in thickness from the bulk gouge layer is almost technically impossible. However, for the purpose of understanding how shear deformation may affect the flash weakening process (our main concern), the use of $T_{d0}|_{\alpha=0.05}$ of the uniformly mixed sample as T_w may naturally consider the more significant mechanochemical changes of the slip-zone materials. This is because the first 5% weight loss of the mixed sample may be mainly attributed to the decomposition of the highly-sheared portions in the gouge layer (i.e., slip-zone materials) that experience the most severe mechanochemical changes.

4.2. Numerical modeling revealing shear-assisted flash weakening and thermochemical pressurization in chlorite-bearing faults

Recent studies have updated the thermochemical pressurization modeling (e.g., Brantut et al., 2010; Chen et al., 2013; Tanikawa et al., 2009) by incorporating the kinetic parameters of decomposition reactions measured for the deformed samples into the modeling (Hirono et al., 2013; Kim et al., 2021). Here we incorporate the intrinsic friction coefficient predicted by flash heating model into the thermochemical pressurization modeling.

The flash heating model predicts that the dynamic weakening may occur due to thermal degradation of the strength of asperity contacts if the characteristic weakening temperature can be achieved on the contacts within their lifetime (Beeler et al., 2008; Goldsby and Tullis, 2011; Rice, 2006). The original flash heating

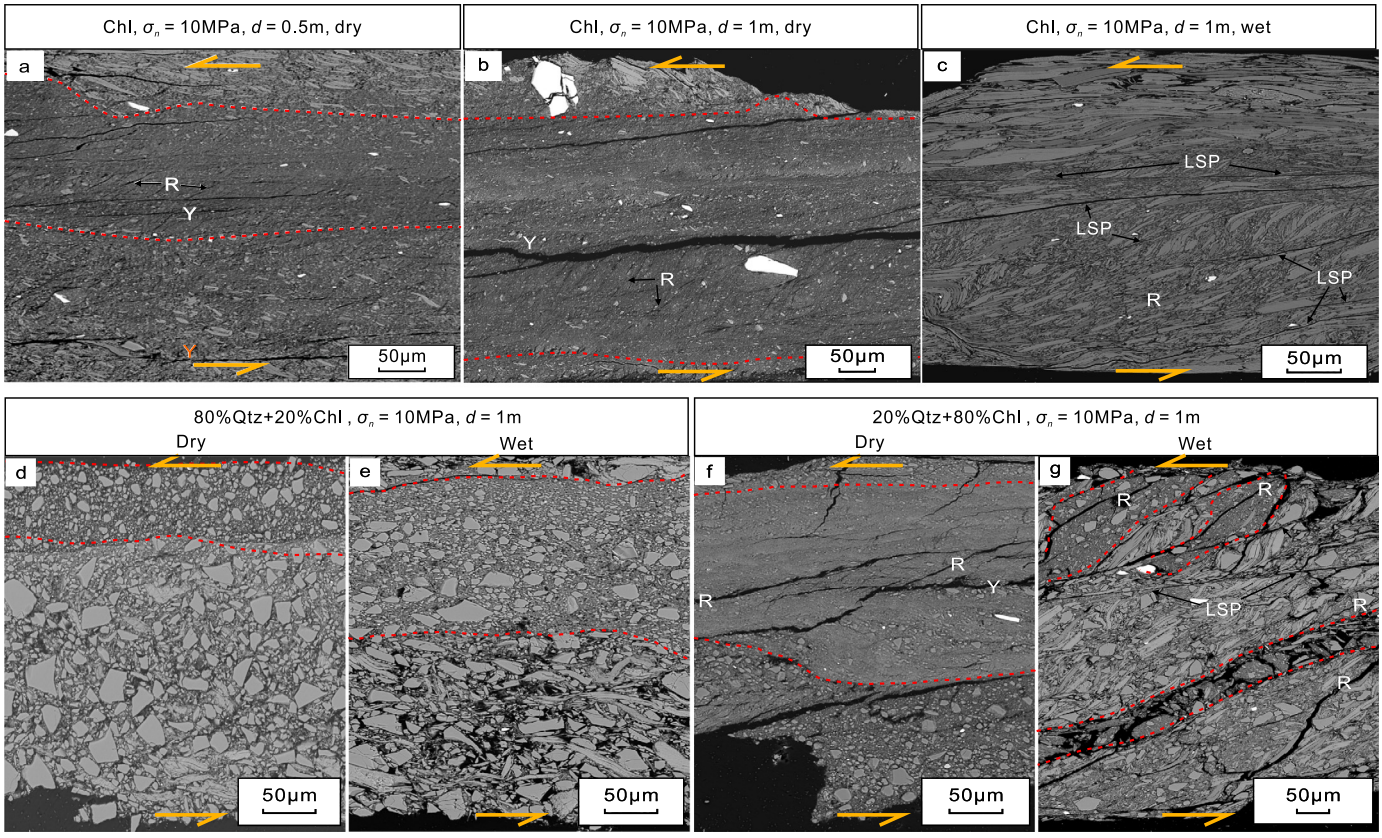

Fig. 5. Microstructures of the sheared chlorite (a–c) and chlorite-quartz mixtures (d–g). The experimental conditions under which the sample was deformed are marked above each image. Abbreviations are R, Riedel shear; Y, Y shear; LSP, localized shear plane.

model is developed for the bare slip surface (Rice, 2006). By considering that the asperity contact may reach the weakening temperature within its lifetime if the slip rate is high enough, Rice (2006) suggests the existence of a characteristic weakening velocity, V_w^{BS}, above which the heat cannot be transferred away fast enough and the flash weakening can be activated,

$$V_w^{BS} = \frac{\pi \alpha_{th}}{D_a}\left[\frac{\rho c\left(T_w - T_f\right)}{\tau_c}\right]^2. \tag{2}$$

Here α_{th} is the thermal diffusivity, ρ is the rock density, c is the heat capacity, D_a is the asperity size, T_w is the weakening temperature (as we discussed in the introduction section), T_f is the average temperature of the fault surface, and τ_c is the contact shear strength. Recent theoretical analysis and experimental results suggest that the T_f and its evolution during fault slip may affect the flash weakening process (Brantut and Platt, 2017; Nielsen et al., 2021; Passelègue et al., 2014; Platt et al., 2014; Proctor et al., 2014; Yao et al., 2016). Moreover, the relatively more distributed shear deformation in the gouge layer than the bare surface is thought to lower the efficiency of flash weakening as the slip rate on a single contact could be reduced (Brantut and Platt, 2017; Platt et al., 2014; Proctor et al., 2014; Yao et al., 2016). The weakening velocity V_w^g in this case is,

$$V_w^g = N_{con} V_w^{BS}, \tag{3}$$

where N_{con} is the number of contacts mobilized across the gouge layer to share the total slip rate. The friction coefficient can be expressed as (Rice, 2006),

$$\begin{cases} \mu = \mu_0, V \le V_w^g, & (4) \\ \mu = (\mu_0 - \mu_w)\dfrac{V_w^g}{V} + \mu_w, V > V_w^g, & (5) \end{cases}$$

where μ_0 is the steady-state friction coefficient at low velocities (as listed in Table S1) and μ_w is the friction coefficient in the weakened state. The μ given by Eqs. (4) and (5) is used as the intrinsic friction coefficient in the modeling of thermochemical pressurization, which is a much better treatment as compared to the assumption of a small constant value (e.g., 0.1) in many previous studies. The measured steady-state friction coefficient was taken as μ_0, and the calculated temperature in the modeling was used as background fault temperature.

From Eqs. (2)–(5), it is clear that all the involved parameters may affect the flash weakening process. Previous work has discussed the uncertainties and variations of the micromechanical and thermal parameters in Eq. (2) and their influence on flash heating (e.g., Passelègue et al., 2014; Tullis, 2015). As we mentioned above, the importance of T_f and N_{con} in the flash weakening has also been stressed in many previous studies. Here we emphasize that the possible reduction in T_w, as suggested by the significantly reduced T_{d0} with increasing mechanical work (Figs. 3a–d and 6b), may promote the flash weakening process. In our view, taking T_{d0} as T_w is plausible. This is not only what scientists in the fault mechanics community commonly use (e.g., Kohli et al., 2011; Tisato et al., 2012; Tullis, 2015), but also a fair inference from the physico-chemical processes associated with thermal decomposition. The causes responsible for the asperity weakening amid thermal decomposition of chlorite may include the volume reduction, the formation of water film (e.g. Sammis et al., 2011), and the

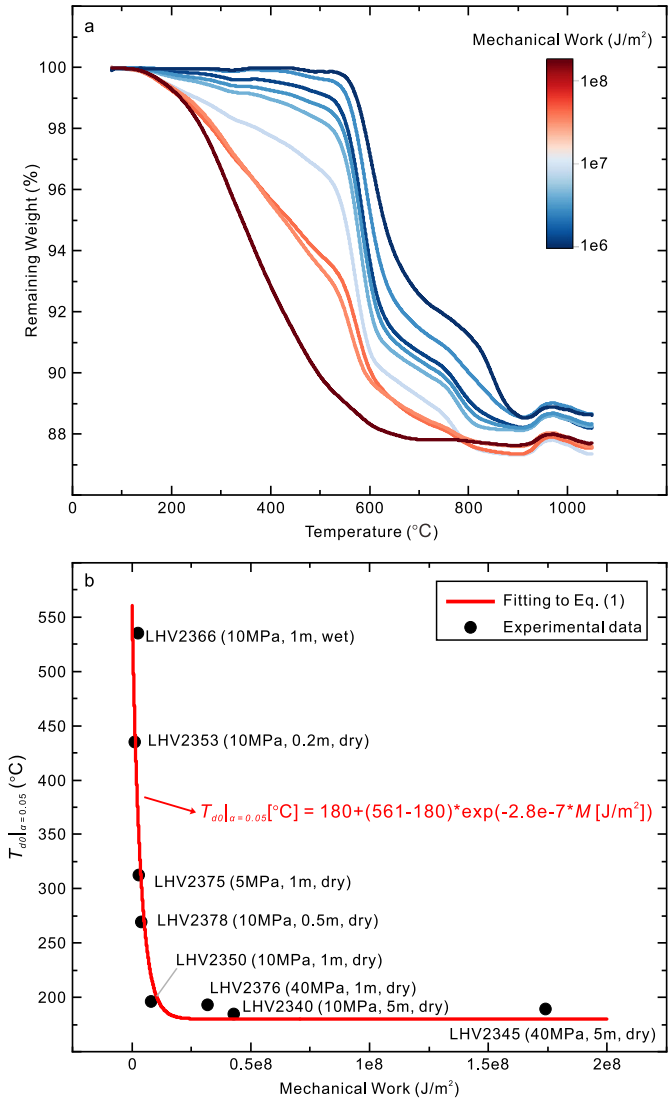

Fig. 6. Variations in the thermal decomposition process and the characteristic temperature with the mechemical work (M) done during shear deformation. (a) Compiled thermogravimetric data. (b) Characteristic temperature (T_{d0}) at which the decomposed fraction reaches 0.05. The relation between T_{d0} and M can be described by Eq. (1). (For interpretation of the colors in the figure(s), the reader is referred to the web version of this article.)

enhanced viscous deformation (e.g. Pozzi et al., 2021) associated with the formation of nanoparticles. Actually, the observed lower peak friction and quicker weakening of the sheared chlorite samples during high-velocity friction experiments may act as indirect evidence to underpin the assumption of $T_{d0} = T_w$. Validating $T_{d0} = T_w$ in the lab seems to be a tough job worthy of exploring in the future. A feasible approach is probably to measure the flash temperature on highly-stressed asperities during friction experiments by infrared thermography (e.g., Sutter and Ranc, 2010; Aretusini et al., 2021), and check whether the average asperity temperature during the early stage of fault weakening may coincide with T_{d0}.

Fig. 6b shows how T_{d0} (T_w) of chlorite may evolve with fault slip. In nature, we believe such evolution of T_w in chlorite-bearing faults mainly occurs during the preslip or the acceleration of coseismic slip (rather than the interseismic stage), when the shear-induced distortion may overtake the recrystallization of the deformed materials. In the modeling, the evolution of T_w with displacement is estimated by the relation between T_{d0} and mechanical work (Eq. (1) and Fig. 6b). N_{con} may also evolve fast especially in the inception of slip, but little is known about its relation with displacement (or time). We simply assume a constant N_{con} of 30 based on the microstructural analysis and the constraints suggested by previous studies (e.g., Rice, 2006; section 1.1). Despite the uncertainties in the estimate of N_{con}, this parameter only affects V_w^g at the very beginning of fault slip. This is because the term $(T_w - T_f)^2$ in Eq. (2) would reduce remarkablely as soon as T_f increases sharply, which would become the most decisive factor in controlling V_w^g in the slip.

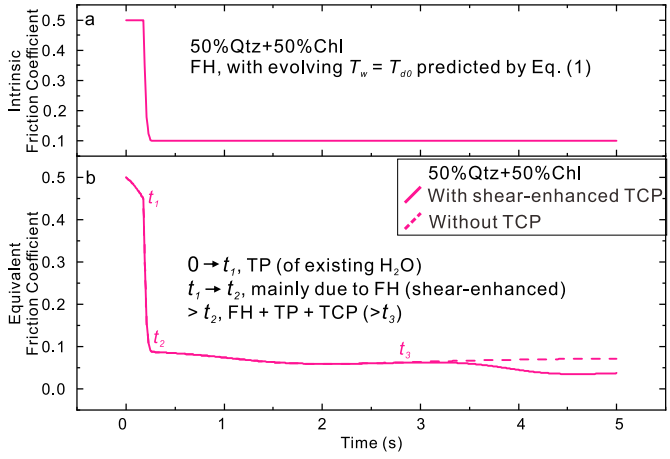

Fig. 7. Predicted dynamic weakening of chlorite-quartz mixture (50% chlorite) by flash heating (FH) and thermochemical pressurization (TCP) under conditions representative of those at 3 km depth. (a), the intrinsic friction coefficient predicted by the FH model. (b) the equivalent friction coefficient predicted by both the FH and TCP models. The effects of shear deformation on the characteristic weakening temperature T_w (= T_{d0}) and the kinetics of thermal decomposition of chlorite are considered in the modeling. The evolution of T_w (T_{d0}) with slip is estimated based on the data shown in Fig. 6b.

The governing equations of thermochemical pressurization are heat and fluid mass conservation equations (Lachenbruch, 1980; Rice, 2006; Brantut et al., 2010; Tanikawa et al., 2009). We assume all the frictional work is converted into heat, and consider the decomposition reaction absorbs heat, releases fluid and reduces the solid volume (increases pore volume). Moreover, we ignore the inelastic porosity changes due to grain crushing, and dilatancy and compaction associated with the granular flow. Then the governing equations are given by (Brantut et al., 2010; Tanikawa et al., 2009; Sulem and Famin, 2009; Platt et al., 2015):

$$\rho c \frac{\partial T}{\partial t} = \nabla \cdot (\lambda \nabla T) + Q_{fric} - Q_{reac} \tag{6}$$

$$S_s \frac{\partial P}{\partial t} = \nabla \cdot \left(\frac{k}{\eta} \nabla P \right) + \varphi \left(\alpha_f - \alpha_m \right) \frac{\partial T}{\partial t} + \Omega_{reac}. \tag{7}$$

Here T is the temperature, t is the time, λ is the thermal conductivity, Q_{fric} is the rate of heat source per unit volume generated by the frictional slip, and Q_{reac} is the rates of heat consumption per unit volume by the chemical reaction. In Eq. (7), P is the pressure, S_s is the specific storage, k is the permeability, η is the dynamic viscosity of the fluid, α_f and α_m are the thermal expansivity of water and grain matrix, respectively, Ω_{reac} is the rate of fluid generation per unit volume by the chemical reaction. As the water-saturated gouge layer consists of both rock powders and pore water, ρ, c and λ used here are equivalent values estimated by either volumetric average (ρ and c) or geometric mean (λ) of those of the component minerals and pore water. Q_{fric} and Q_{reac} in Eqs. (6) and (7) can be found as:

$$Q_{fric} = \frac{\mu \left(\sigma_n - P_{ave} \right) V}{w}, \tag{8}$$

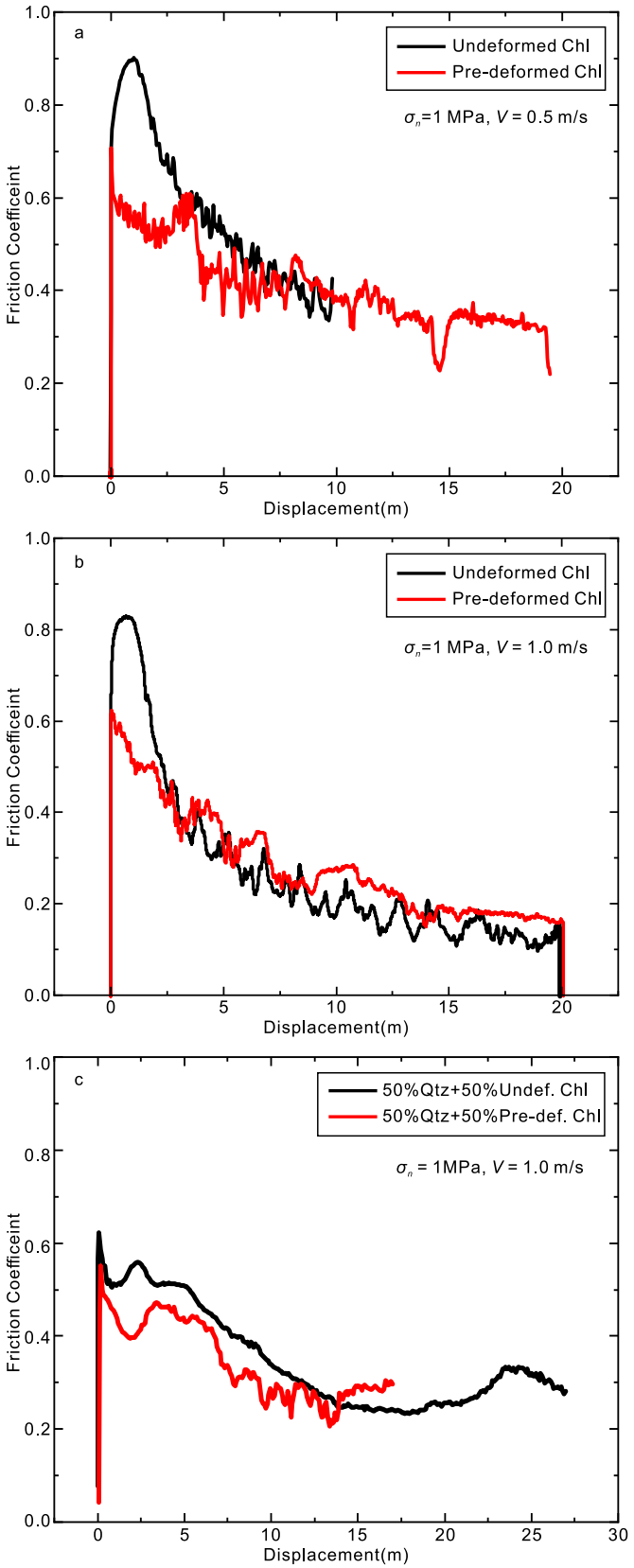

Fig. 8. Friction coefficient as a function of displacement recorded in high-velocity experiments conducted on undeformed and pre-deformed chlorite and chlorite-quartz samples under room-humidity condition. Normal stress (σ_n) is 1.0 MPa in all the experiments and slip rate (V) is either 0.5 or 1.0 m/s. In consideration of a few scientific and technical issues (discussed in the text), the pre-deformed samples were prepared by using a planetary ball mill.

$$Q_{reac} = w_{reac}\,(1-\varphi)\,\rho\,\Delta H\frac{\partial\alpha}{\partial t}, \tag{9}$$

respectively. Here V is the slip rate, σ_n is the normal stress, μ is the intrinsic friction coefficient (estimated using the flash heating model), w is the shear-zone thickness, and P_{ave} is the mean pore pressure in the shear zone (Sulem and Famin, 2009) defined as $P_{ave} = \int_{-w/2}^{w/2} P\,(x)\,dx/w$. In Eq. (9), w_{reac} is the content of reactant (chlorite here) in the sample, φ is the porosity, ΔH and $(\partial\alpha/\partial t)$ are the enthalpy and kinetics of the reaction (obtainable by the STA analysis as described in the Supplemental Material). The specific storage S_s in Eq. (6) is defined as (Wibberley and Shimamoto, 2005):

$$S_s = \beta_b + \varphi\beta_f - (1+\varphi)\,\beta_m, \tag{10}$$

where β_b, β_f and β_m are the compressibilities of the bulk gouge layer, the pore water and the mineral grain matrix, respectively. Assuming that the reaction changes 1 mol of reactant to 1 mol of decomposition product and χ mol of fluid, the rate of fluid generation per unit volume is given by (Chen et al., 2013; Hirono et al., 2013; Tanikawa et al., 2009):

$$\Omega_{reac} = w_{reac}\,(1-\varphi)\left(\frac{\chi M_f}{\rho_f}\frac{\rho_{reac}}{M_{reac}} + \frac{M_{prod}}{\rho_{prod}}\frac{\rho_{reac}}{M_{reac}} - 1\right)\frac{\partial\alpha}{\partial t}, \tag{11}$$

where M_f and ρ_f, M_{reac} and ρ_{reac}, and M_{prod} and ρ_{prod} are the molar masses and densities of the released water, the reactant (chlorite here) and the solid phase of the decomposition product, respectively. $(\frac{\chi M_f}{\rho_f}\frac{\rho_{reac}}{M_{reac}})$ represents the ratio of the molar volume of the released fluid to that of the reactant, while $(\frac{M_{prod}}{\rho_{prod}}\frac{\rho_{reac}}{M_{reac}} - 1)$ refers to the solid volume reduction (%) caused by the reaction. If we assume $\rho_{reac} \approx \rho_{prod}$, and consider $(\chi M_f\,/M_{reac})$ can be estimated as the weight loss ratio w_{loss} (the weight ratio of the released fluid to the reactant) from the TG data, Eq. (11) can be rearranged as:

$$\Omega_{reac} = w_{reac}\,(1-\varphi)\,w_{loss}\left(\frac{\rho_{reac}}{\rho_f} - 1\right)\frac{\partial\alpha}{\partial t}. \tag{12}$$

The equivalent friction coefficient (μ_{eq}) with the consideration of both flash heating and thermochemical pressurization then can be given as:

$$\mu_{eq} = \frac{\mu\,(\sigma_n - P_{ave})}{\sigma_n}, \tag{13}$$

where μ is the intrinsic friction coefficient predicted by the flash weakening (Eqs. (4) and (5)). We solve the above equations with a one-dimension geometric model in Comsol Multiphysics. We consider a 10 mm thick gouge zone sandwiched by two breccia zones with the thickness of 100 mm and 400 mm, respectively, on each side (Fig. S8a in Supplemental Material; see information about boundary conditions and mesh model in the paragraph above Fig. S8). The environmental conditions represent those at a depth of 3 km. All the relevant properties utilized in the modeling are summarized in Table S3 in Supplemental Material.

We think all the relevant parameters determined for the chlorite-quartz mixtures sheared under wet conditions may better reflect those for natural fault zones (in terms of mineral composition and fluid conditions). We here present the modeling results for the cases of the chlorite-quartz mixtures with 50% chlorite (Fig. 7; see all the parameters used in Table S2 (LHV2475) and S3). As the initial threshold velocity of flash weakening is much higher than the slip rate (V) due to distributed shear (see Eqs. (2)

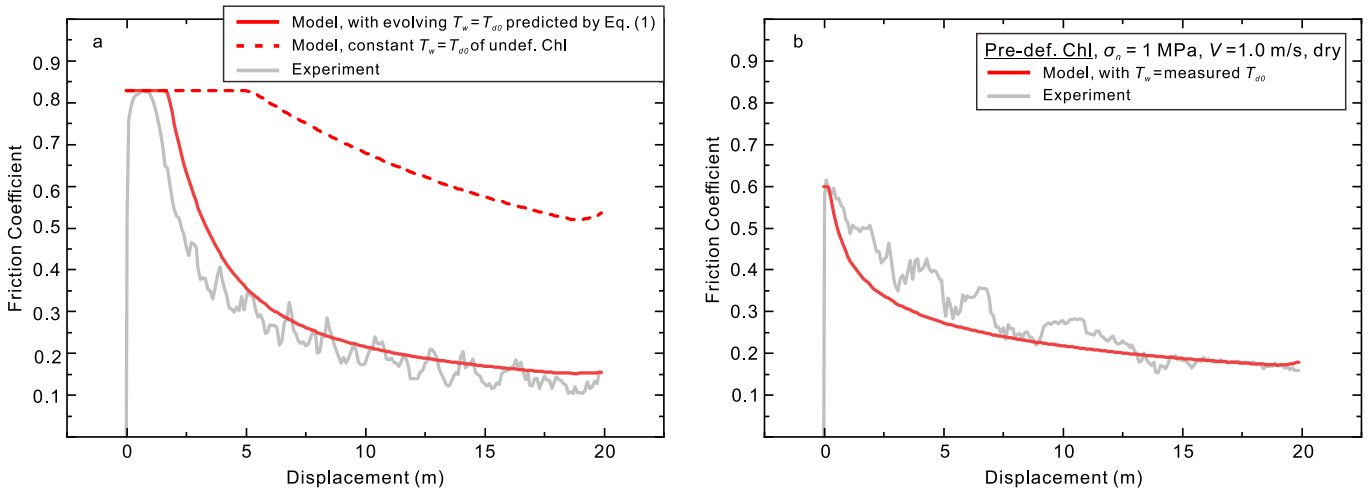

Fig. 9. Evolution of friction with displacement predicted by flash weakening and thermochemical pressurization. Solid gray: experimental data; solid red: model prediction incorporating the shear-induced reduction in T_w (T_{d0}); dashed gray: model prediction using constant T_w (T_{d0} of the undeformed chlorite sample).

and (3)), the intrinsic friction coefficients predicted by flash heating remain high at the beginning (Fig. 7a). Flash weakening occurs as fault temperature T_f(t) goes up toward T_w to reduce V_w (t) to a value lower than V (see Eq. (2)). The faster flash weakening can be expected for a lower T_w (Fig. 7a). The equivalent friction coefficient predicted by both flash heating (FH) and thermochemical pressurization (TCP) shows that the thermal pressurization of existing pore water (TP) dominates the weakening process in the very beginning ($t < t_1$; Fig. 7b) until it is soon overtaken by FH ($t_1 < t < t_2$). The shear-enhanced TCP takes effect in the later stage, adding an extra fault weakening ($t > t_3$; Fig. 7b; cp. the dashed and solid lines; Fig. S9 in Supplemental Material).

4.3. High-velocity friction experiments revealing mechanochemical effects on dynamic weakening of chlorite-bearing samples

To corroborate the mechanochemical effects on dynamic weakening of chlorite-bearing samples, a rational way is to conduct high-velocity friction experiments on pre-sheared and unsheared samples, and compare the observed frictional behaviors. One may think that we can simply shear chlorite samples via low-velocity friction experiments and then continue to do high-velocity tests on the sheared samples. However, this would involve another crucial factor, the degree of shear localization, in the comparison. The logic is that the presheared samples typically have shorter weakening distance in high-velocity friction experiments than the solely compacted samples, for which the differences in the shear texture and the degree of localization are plausible causes. An approach to exclude this influence is to disaggregate the presheared gouge layer to remove the shear texture and then mount the gouges again for high-velocity tests. Moreover, the sample assembly used in our low-velocity experiments allows the imposition of high normal stress, but the top speed is currently limited to ~10 mm/s (Fig. S1a). The assembly used in the high-velocity friction experiments requires more samples (2.5 g) than those in the low-velocity tests (1.0 g). Considerating all these scientific and technical issues, we use a planetary ball mill to prepare the deformed samples for the high-velocity experiments, which is much more efficient in practice. The STA and XRD analyses have confirmed that the deformed samples prepared in this way are quite akin to those experimentally sheared (Fig. S2).

Fig. 8 presents the results from high-velocity friction experiments performed on the undeformed and pre-deformed chlorite-bearing samples under V = 0.5–1.0 m/s and σ_n = 1 MPa. For the nearly pure chlorite, the frictional behaviors of the undeformed and pre-deformed samples are quite different in the first 3–4 m of slip, after which the friction curves almost overlap (Figs. 8a and b). For the undeformed sample, it is clear that a peak friction coefficient of 0.83 appears after sliding for 0.69 m at V = 1.0 m/s, followed by a rapid weakening (Fig. 8b). In contrast, a smaller peak friction coefficient of 0.62 appears almost at the onset of slip (~0.03 m) for the pre-deformed sample (Fig. 8b). The area enclosed by the two curves at d < 3 m multiplied by the applied σ_n gives an estimate of the difference in specific fracture energy of 0.659 MJ/m^2 between the two samples. The visibly lower fracture energy of the pre-deformed sample during high-velocity sliding suggests that shear deformation of fault-zone materials may help promote rupture propagation during earthquakes. For the quartz-chlorite mixture, both the peak friction and the overall friction level in the first 12 m of slip are lower for the pre-deformed sample (Fig. 8c), roughly consistent with the results of the nearly pure chlorite.

A plausible explanation of what we observed in high-velocity friction experiments is that flash weakening in the pre-deformed chlorite can be significantly promoted in the early stage of slip due to the lowered T_w, as suggested by the significantly lowered T_{d0} with increasing mechanical work (Fig. 6b). One may question whether the reduction in grain size and the existence of amorphous materials in the pre-deformed samples may lower the overall friction level in the first a few meters of slip. However, this can be excluded by the observed high friction throughout the low-velocity (1 mm/s) friction experiment with a final displacement of 5 m (Fig. 1a).

We here perform additional modeling to check whether we could reproduce the observed experimental results as shown in Fig. 8b. We solve the Eqs. (2)–(12) with a 2-D axisymmetric finite element model using Comsol Multiphysics. The geometric model is built based on the real sample assembly used in the high-velocity friction experiments (Fig. S1b and Fig. S8b in Supplemental Material). For the milled sample, since the measured T_{d0} is already very close to the fitted T_{d0_inf} (Eq. (1)), we simply set T_w as a constant value equaling the measured T_{d0}. For the undeformed sample, the evolution of T_w with displacement is considered based on the fitting results shown in Fig. 6b. μ_0 of the two samples (see Eq. (2)) are set as the measured peak friction coefficients. N_{con} is set as 10 in consideration of the thin gouge layer of ~1.0–1.5 mm in the experiments. In addition, as the initial pore fluid is air in the experiments and the released water by thermal decomposition must be in vapor phase, we simply take the pore fluid as air to avoid the complexities of two-phase flow. The physical properties of the host

blocks and the confining Teflon ring are quoted from those used in Yao et al. (2016). All other parameters are exactly same as those used in the modeling for the fault-zone model at 3 km depth (Table S3 in Supplemental Material). Because of the gradient of the slip velocity (thus also the temperature and pore pressure) on the circular slip surface, μ_{eq} can be expressed in a different form by simple derivation (Eq. (S10) in Supplemental Material).

The modeling results shown in Fig. 9 demonstrate the role of the lowered T_w (= T_{d0}) in the dynamic weakening of chlorite gouges. By incorporating the shear-induced reduction in T_w, the modeling results (red curves) and the experimental data (solid gray curves) show reasonably good agreement (Fig. 9). In contrast, flash heating and thermochemical pressurization are inadequate to cause the observed weakening when T_w is kept as high as T_{d0} of the undeformed chlorite (561 °C; dashed red curves). As there are a number of decisive parameters that may affect the modeling results (e.g., N_{con}, τ_c, D_a, and the permeability of the sheared gouge layer and the sealing capability of Teflon sleeve, etc), we cannot assert that the modeling with constant T_w is totally impossible to reproduce the measured frictional behavior. However, the results shown in Fig. 9 clearly demonstrate that T_w and its changes with shear deformation could play a crucial role in dynamic fault weakening.

5. Conclusion

Our results highlight the interaction between shear deformation and fault weakening during seismic slip, as firstly stressed in Hirono et al. (2013). New findings in this study are that shear deformation may not only facilitate thermochemical pressurization (Hirono et al., 2013; Kim et al., 2021) but also aid in flash weakening through the markedly reduced T_w. We may expect that the accelerating slip in the initiation of coseismic faulting could distort the slip-zone materials, making the activation of both flash weakening and thermochemical pressurization (especially the former) much quicker and easier. The resultant lower friction and fracture energy may in turn promote fault slip and rupture propagation. Currently, such mechanochemical effects on fault weakening are only examined for a few minerals, and more work is required for other thermally-unstable minerals and rocks in the future.

CRediT authorship contribution statement

Bowen Yu: Data curation, Formal analysis, Investigation, Methodology, Writing – original draft, Writing – review & editing. **Lu Yao:** Conceptualization, Data curation, Formal analysis, Funding acquisition, Investigation, Methodology, Supervision, Writing – original draft, Writing – review & editing. **Shengli Ma:** Formal analysis, Funding acquisition, Supervision, Writing – review & editing. **Weifeng Qin:** Data curation, Methodology.

Declaration of competing interest

The authors declare that they have no known competing financial interests or personal relationships that could have appeared to influence the work reported in this paper.

Data availability

Data will be made available on request.

Acknowledgements

This study was supported by the Institute of Geology, China Earthquake Administration (grant IGCEA2107 to L.Y.), the National Natural Science Foundation of China (grant U1839211 to S.M. and grants 42111530030 and 42174223 to L.Y.), and the National Key R&D Program of China (2021YFC3000603-04). We are grateful to Xi Ma and Qingbao Duan for their help in sample preparation and microstructural observation, and Yong Xue for his help in XRD analysis. The authors acknowledge the Editor R. Bendick, one anonymous reviewer and Xiaofeng Chen for their constructive comments.

Appendix A. Supplementary material

Supplementary material related to this article can be found online at https://doi.org/10.1016/j.epsl.2022.117971.

References

Aretusini, S., Núñez-Cascajero, A., Spagnuolo, E., Tapetado, A., Vázquez, C., Di Toro, G., 2021. Fast and localized temperature measurements during simulated earthquakes in carbonate rocks. Geophys. Res. Lett. 48, e2020GL091856. https://doi.org/10.1029/2020GL091856.

Arkhangel'Skii, I., Dunaev, A., Makarenko, I., Tikhonov, N., Belyaev, S., Tarasov, A., 2013. Non-isothermal kinetic methods. Workbook and laboratory manual. Max Planck research library for the history and development of knowledge. Germany: Edition Open Access Berlin.

Beeler, N.M., Tullis, T.E., Goldsby, D.L., 2008. Constitutive relationships and physical basis of fault strength due to flash heating. J. Geophys. Res. 113. https://doi.org/10.1029/2007jb004988.

Bourdelle, F., Cathelineau, M., 2015. Low-temperature chlorite geothermometry: a graphical representation based on a T–R2+–Si diagram. Eur. J. Mineral. 27, 617–626.

Brantut, N., Platt, J.D., 2017. Dynamic weakening and the depth dependence of earthquake faulting. In: Thomas, M.Y., Mitchell, T.M., Bhat, H.S. (Eds.), Fault Zone Dynamic Processes: Evolution of Fault Properties During Seismic Rupture. Washington, D. C. In: Geophys. Monogr. Ser., pp. 171–194.

Brantut, N., Schubnel, A., Corvisier, J., Sarout, J., 2010. Thermochemical pressurization of faults during coseismic slip. J. Geophys. Res. 115, B05314. https://doi.org/10.1029/2009jb006533.

Chen, J., Yang, X., Yao, L., Ma, S., Shimamoto, T., 2013. Frictional and transport properties of the 2008 Wenchuan Earthquake fault zone: implications for coseismic slip-weakening mechanisms. Tectonophysics 603, 237–256. https://doi.org/10.1016/j.tecto.2013.05.035.

Di Toro, G., Han, R., Hirose, T., De Paola, N., Nielsen, S., Mizoguchi, K., Ferri, F., Cocco, M., Shimamoto, T., 2011. Fault lubrication during earthquakes. Nature 471, 494–498. https://doi.org/10.1038/nature09838.

Földvári, M., 2011. Handbook of Thermogravimetric System of Minerals and Its Use in Geological Practice. Geological Institute of Hungary Budapest.

Friedman, H.L., 1964. Kinetics of thermal degradation of char-forming plastics from thermogravimetry. Application to a phenolic plastic. J. Polym. Sci. Part C 6 (1), 183–195.

Goldsby, D.L., Tullis, T.E., 2011. Flash heating leads to low frictional strength of crustal rocks at earthquake slip rates. Science 334, 216–218. https://doi.org/10.1126/science.1207902.

Hirono, T., Tanikawa, W., 2011. Implications of the thermal properties and kinetic parameters of dehydroxylation of mica minerals for fault weakening, frictional heating, and earthquake energetics. Earth Planet. Sci. Lett. 307, 161–172. https://doi.org/10.1016/j.epsl.2011.04.042.

Hirono, T., Tanikawa, W., Honda, G., Kameda, J., Fukuda, J.-i., Ishikawa, T., 2013. Importance of mechanochemical effects on fault slip behavior during earthquakes. Geophys. Res. Lett. 40, 2988–2992. https://doi.org/10.1002/grl.50609.

Kaneki, S., Oohashi, K., Hirono, T., Noda, H., 2020. Mechanical amorphization of synthetic fault gouges during rotary-shear friction experiments at subseismic to seismic slip velocities. J. Geophys. Res. 125, e2020JB019956. https://doi.org/10.1029/2020jb019956.

Kim, H.N., So, B.-D., Kim, M.S., Han, K.S., Oh, S.B., 2021. Seismic fault weakening via CO2 pressurization enhanced by mechanical deformation of dolomite fault gouges. Geology 49 (10), 1245–1249. https://doi.org/10.1130/g48938.1.

Kohli, A.H., Goldsby, D.L., Hirth, G., Tullis, T., 2011. Flash weakening of serpentinite at near-seismic slip rates. J. Geophys. Res. 116, B03202. https://doi.org/10.1029/2010JB007833.

Lachenbruch, A.H., 1980. Frictional heating, fluid pressure, and the resistance to fault motion to fault motion. J. Geophys. Res. 85 (B11), 6097–6112. https://doi.org/10.1029/JB085iB11p06097.

Ma, S., Shimamoto, T., Yao, L., Togo, T., Kitajima, H., 2014. A rotary-shear low to high-velocity friction apparatus in Beijing to study rock friction at plate to seismic slip rates. Earthq. Sci. 27, 469–497. https://doi.org/10.1007/s11589-014-0097-5.

Masumoto, H., Kameda, J., Arima, H., Sugiyama, K., Nagai, T., Yamamoto, Y., 2018. Dehydroxylation kinetics of clay minerals and its application to friction heating along an imbricate thrust in an accretionary prism. Geochem. Geophys. Geosyst. 19, 2991–3003. https://doi.org/10.1029/2018GC007472.

Molinari, A., Estrin, Y., Mercier, S., 1999. Dependence of the coefficient of friction on the sliding conditions in the high velocity range. J. Tribol. 121, 35–41. https://doi.org/10.1115/1.2833808.

Nielsen, S., Spagnuolo, E., Violay, M., Di Toro, G., 2021. Thermal weakening friction during seismic slip: experiments and models with heat sources and sinks. J. Geophys. Res. 126, e2020JB020652. https://doi.org/10.1029/2020JB020652.

Noda, H., Lapusta, N., 2010. Three-dimensional earthquake sequence simulations with evolving temperature and pore pressure due to shear heating: effect of heterogeneous hydraulic diffusivity. J. Geophys. Res. 115, B12314. https://doi.org/10.1029/2010jb007780.

Noda, H., Lapusta, N., 2013. Stable creeping fault segments can become destructive as a result of dynamic weakening. Nature 493, 518–521. https://doi.org/10.1038/nature11703.

Passelègue, F.X., Goldsby, D.L., Fabbri, O., 2014. The influence of ambient fault temperature on flash-heating phenomena. Geophys. Res. Lett. 41, 828–835. https://doi.org/10.1002/2013GL058374.

Platt, J., Proctor, B., Mitchell, T., Hirth, G., Goldsby, D., Di Toro, G., Beeler, N., Tullis, T., 2014. The role of gouge and temperature on flash heating and its hysteresis. In: AGU Fall Meeting Abstracts, p. 4360.

Platt, J.D., Brantut, N., Rice, J.R., 2015. Strain localization driven by thermal decomposition during seismic shear. J. Geophys. Res. 120, 4405–4433. https://doi.org/10.1002/2014JB011493.

Pozzi, G., De Paola, N., Nielsen, S.B., Holdsworth, R.E., Tesei, T., Thieme, M., Demouchy, S., 2021. Coseismic fault lubrication by viscous deformation. Nat. Geosci. 14, 437–442. https://doi.org/10.1038/s41561-021-00747-8.

Proctor, B.P., Mitchell, T.M., Hirth, G., Goldsby, D., Zorzi, F., Platt, J.D., Di Toro, G., 2014. Dynamic weakening of serpentinite gouges and bare surfaces at seismic slip rates. J. Geophys. Res. 119, 2014JB011057. https://doi.org/10.1002/2014JB011057.

Rice, J.R., 2006. Heating and weakening of faults during earthquake slip. J. Geophys. Res. 111, B05311. https://doi.org/10.1029/2005jb004006.

Reches, Z.e., Lockner, D.A., 2010. Fault weakening and earthquake instability by powder lubrication. Nature 467, 452–455. https://doi.org/10.1038/nature09348.

Rubino, V., Lapusta, N., Rosakis, A.J., 2022. Intermittent lab earthquakes in dynamically weakening fault gouge. Nature 606, 922–929. https://doi.org/10.1038/s41586-022-04749-3.

Sammis, C., Lockner, D., Reches, Z.e., 2011. The role of adsorbed water on the friction of a layer of submicron particles. Pure Appl. Geophys. 168, 2325–2334. https://doi.org/10.1007/s00024-011-0324-0.

Scholz, C., 2002. The Mechanics of Earthquakes and Faulting, 2nd ed. Cambridge University Press, Cambridge.

Shimamoto, T., Tsutsumi, A., 1994. A new rotary-shear high-speed frictional testing machine: its basic design and scope of research. J. Tecton. Res. Group Jpn. 39, 65–78 (in Japanese with English abstract).

Spagnuolo, E., Plümper, O., Violay, M., Cavallo, A., Di Toro, G., 2015. Fast-moving dislocations trigger flash weakening in carbonate-bearing faults during earthquakes. Sci. Rep. 5, 16112. https://doi.org/10.1038/srep16112.

Steudel, A., Kleeberg, R., Koch, C.B., Friedrich, F., Emmerich, K., 2016. Thermal behavior of chlorites of the clinochlore-chamosite solid solution series: oxidation of structural iron, hydrogen release and dehydroxylation. Appl. Clay Sci. 132–133, 626–634. https://doi.org/10.1016/j.clay.2016.08.013.

Sulem, J., Famin, V., 2009. Thermal decomposition of carbonates in fault zones: slip-weakening and temperature-limiting effects. J. Geophys. Res. 114. https://doi.org/10.1029/2008JB006004.

Sutter, G., Ranc, N., 2010. Flash temperature measurement during dry friction process at high sliding speed. Wear 268, 1237–1242. https://doi.org/10.1016/j.wear.2010.01.019.

Tanikawa, W., Sakaguchi, M., Hirono, T., Lin, W., Soh, W., Song, S.-R., 2009. Transport properties and dynamic processes in a fault zone from samples recovered from TCDP Hole B of the Taiwan Chelungpu Fault Drilling Project. Geochem. Geophys. Geosyst. 10, Q04013. https://doi.org/10.1029/2008gc002269.

Tisato, N., Di Toro, G., De Rossi, N., Quaresimin, M., Candela, T., 2012. Experimental investigation of flash weakening in limestone. J. Struct. Geol. 38, 183–199. https://doi.org/10.1016/j.jsg.2011.11.017.

Tullis, T.E., 2015. Mechanisms for friction of rock at earthquake slip rates. In: Schubert, G. (Ed.), Treatise on Geophysics, second edition. Elsevier, Oxford, pp. 139–159.

Vyazovkin, S., Chrissafis, K., Di Lorenzo, M.L., Koga, N., Pijolat, M., Roduit, B., Sbirrazzuoli, N., Suñol, J.J., 2014. ICTAC Kinetics Committee recommendations for collecting experimental thermal analysis data for kinetic computations. Thermochim. Acta 590, 1–23. https://doi.org/10.1016/j.tca.2014.05.036.

Wibberley, C.A.J., Shimamoto, T., 2005. Earthquake slip weakening and asperities explained by thermal pressurization. Nature 436, 689–692. https://doi.org/10.1038/nature03901.

Yao, L., Ma, S., Platt, J.D., Niemeijer, A.R., Shimamoto, T., 2016. The crucial role of temperature in high-velocity weakening of faults: experiments on gouge using host blocks with different thermal conductivities. Geology 44, 63–66. https://doi.org/10.1130/g37310.1.